JOURNAL OF GUIDANCE, CONTROL, AND DYNAMICS
Vol. 28, No. 3, May–June 2005

Fast In-Flight Detection of Flutter Onset: A Statistical Approach

Laurent Mevel,* Michèle Basseville,† and Albert Benveniste‡
Institut de Recherche en Informatique et Systèmes Aléatoires, 35042 Rennes Cedex, France

The flutter monitoring problem is investigated from a detection (and not prediction) point of view and is stated as a statistical hypotheses testing problem regarding a specified damping coefficient. An on-line flutter onset detection algorithm is described. This test builds on a residual associated with an output-only subspace-based structural identification method, previously introduced by the authors for structural health monitoring. Whereas, in our previous work, the subspace-based residual was covariance driven and the test was based on the asymptotic statistical local approach to monitoring, the on-line test proposed involves a temporal data-driven computation for the subspace-based residual and builds on a different asymptotic, combined with the cumulative sum test of common use in quality control. Numerical results obtained on real data are discussed, which show interesting properties of the on-line test.

Nomenclature

C	=	damping matrix
$\mathcal{C}_q$	=	controllability matrix, with q block columns
$\boldsymbol{E}$	=	expectation operator
F, H	=	$2m \times 2m$ state transition and $r \times 2m$ observation matrices
f	=	frequency (discrete-time model)
g_n, g_n^+, g_n^-	=	cumulative sum test statistics
$\mathcal{H}_{p,q}$	=	Hankel matrix, with p block rows and q block columns
$\boldsymbol{H}_0$, $\tilde{\boldsymbol{H}}_0$	=	null hypothesis for θ (or ρ) and ν, respectively
$\boldsymbol{H}_1$, $\tilde{\boldsymbol{H}}_1$	=	alternative hypothesis for θ (or ρ) and ν, respectively
$\mathcal{I}$	=	sensitivity matrix of $\boldsymbol{\zeta}$ with respect to $\delta\theta$
$\Im$, $\Re$	=	imaginary and real parts, respectively, of a complex number
K, M	=	stiffness and mass matrices
$\mathcal{O}_p$	=	observability matrix, with p block rows
$Q_\varepsilon(t)$, Q_k	=	covariance matrix of $\varepsilon(t)$ and V_k, respectively
R_i	=	lag i covariance matrix of Y
S_n, $S_n^{(+)}$, $S_n^{(-)}$	=	cumulative sums
T_n, $T_n^{(+)}$, $T_n^{(-)}$	=	maximum value of the S_k, $S_k^{(+)}$, and $S_k^{(-)}$, respectively
U	=	$(p+1)\cdot r$ orthogonal matrix
$\boldsymbol{V}_k$, $\boldsymbol{X}_k$	=	discrete-time state noise and state vector
$\boldsymbol{Y}_k$, $\boldsymbol{Y}(t)$	=	discrete- and continuous-time measurement vectors
$\boldsymbol{\mathcal{Y}}_{k,p}^+$, $\boldsymbol{\mathcal{Y}}_{k,q}^-$	=	p future and q past measurement vectors stacked on top of each other
$\boldsymbol{\mathcal{Z}}(t)$	=	vector collecting the displacements of the degrees of freedom of the structure
γ, γ^+, γ^-	=	thresholds for tests g_n, g_n^+, and g_n^-, respectivley
Δ, $\boldsymbol{\Lambda}$	=	diagonal matrix and vector, respectively, filled with the λ
$\delta\boldsymbol{\theta}$	=	deviation in $\boldsymbol{\theta}$
$\varepsilon(t)$	=	continuous-time state noise
$\boldsymbol{\zeta}_n$, $\bar{\boldsymbol{\zeta}}_n$	=	residual vector and scale-normalized residual vector
$\boldsymbol{\theta}$, $\boldsymbol{\theta}_0$	=	modal parameter vector and reference value
λ, μ	=	eigenvalue of F and mode
$\boldsymbol{\nu}$	=	mean value of $\boldsymbol{Z}_k$, an increment of $\bar{\boldsymbol{\zeta}}_n$
ρ, ρ_0, ρ_c	=	damping coefficient, reference value, critical value
Σ, $\bar{\Sigma}$	=	covariance matrix of $\boldsymbol{\zeta}_n$ and $\bar{\boldsymbol{\zeta}}_n$
τ	=	sampling frequency
Φ	=	matrix whose columns are the φ_λ
ϕ_λ, φ_λ	=	eigenvector of F associated with λ, and its observed components
χ_n^2, $\bar{\chi}_n^2$	=	chi-square test associated with $\boldsymbol{\zeta}_n$ and $\bar{\boldsymbol{\zeta}}_n$
Ψ_μ	=	mode shape associated with mode μ
$\hat{}$	=	$\hat{A}$, estimated value of a scalar, vector, or matrix A

Introduction

THE development of new aircrafts requires a careful exploration of the dynamic behavior of the structure subject to vibration and aeroservoelastic forces. This is achieved via a combination of ground vibration tests and in-flight tests. For both types of tests, various sensors' data are recorded, and modal analyses are performed. Important challenges of the in-flight modal analyses are the limited choices for measured excitation inputs and the presence of unmeasured natural excitation input (turbulence). A better exploitation of flight-test data can be achieved by using output-only system identification methods, which exploit data recorded under natural excitation conditions, for example, turbulent, without resorting to artificial control surface excitation and other types of excitation inputs.[1,2]

A crucial issue is to ensure that the newly designed airplane is stable throughout its operating range. A critical instability phenomenon, known as "aero-elastic flutter, involves the unfavorable interaction of aerodynamic, elastic, and inertia forces on structures to produce an unstable oscillation that often results in structural failure."[3] To prevent this phenomenon, the airplane is submitted to a flight flutter testing procedure, with incrementally increasing altitude and airspeed. The problem of predicting the speed at which flutter can occur is usually addressed with the aid of identification methods that achieve modal analysis from the in-flight data recorded during these tests.[3–5] Three different levels are distinguished in Ref. 4. The level 1 approach, basically handling one degree of freedom, counts zero crossings and computes log decrement damping on charts recording impulse decays and captures only a single dominant mode. The level 2 approach uses multiple-degrees-of-freedom methods for estimating global modal estimates (frequencies and damping coefficients) and is necessary when the mode of interest does not dominate the response. The level 3 approach estimates

Received 31 October 2003; revision received 12 March 2004; accepted for publication 12 March 2004.

*Researcher, Institut National de Recherche en Informatique et en Automatique, Campus de Beaulieu.

†Research Director, Centre National de la Recherche Scientifique, Campus de Beaulieu; basseville@irisa.fr.

‡Research Director, Institut National de Recherche en Informatique et en Automatique, Campus de Beaulieu.

aerodynamic parameters and a stability boundary, for flutter stability prediction.[6] The rationale of the first two approaches is that the damping coefficient reflects the rate of increase or decrease in energy in the aeroservoelastic system and, thus, is a relevant measure of stability. Therefore, although frequencies and mode shapes are usually the most important parameters in structural analysis, the most critical ones in flutter analysis are the damping factors, for some critical modes. The mode shapes are usually not estimated for flutter testing.[4]

Until the late 1990s, most approaches to flutter clearance have led to data-based methods, processing different types of data.[5] Many methods handle time-domain or frequency-domain functions, based on responses to impulse excitation or atmospheric turbulence.[3,7,8] A comparison of data from the F-18 SRA, involving modern time- and frequency-domain subspace identification methods, is reported in Ref. 7. A combined data-based and model-based method has been introduced recently called flutterometer.[9] Based on an aeroelastic state-space model and on frequency-domain transfer functions extracted from sensor data under controlled excitation, the flutterometer computes on-line a robust flutter margin using the μ method to analyze the worst-case effects of model uncertainty. In recent comparative evaluations using simulated and real data,[5,6] several data-based methods are shown to fail to predict accurately flutter when using data from low-speed tests, whereas the flutterometer is shown not to converge to the true flutter speed during envelope expansion, due to inherent conservative predictions.

Algorithms achieving the on-line in-flight exploitation of flight-test data are expected to allow a more direct exploration of the flight domain, with improved confidence and reduced costs. Among other challenges, one important issue to be addressed on-line is the flight flutter monitoring problem, stated as the problem of monitoring some specific damping coefficients. However, it is known, for example, from Cramer–Rao bounds (see Ref. 10), that damping factors are difficult to estimate accurately. To improve the estimation of damping factors, and moreover to achieve this in real-time during flight tests, one possible although unexpected route is to rely on detection algorithms able to decide whether some damping factor decreases below some critical value or not. The rationale is that detection algorithms usually have a much shorter response time than identification algorithms.

The purpose of this paper is to describe and analyze a statistical test for monitoring a damping factor. This test is based on a subspace-based residual previously proposed by the authors for both modal identification and structural health monitoring (SHM). The residual is ideally zero under the hypothesis of constant modal parameters (null hypothesis) and significantly different from zero in the presence of a deviation in the parameters, here in a specific damping coefficient (alternative hypothesis). Whereas our residual was covariance driven and our SHM test was based on the asymptotic statistical local approach to monitoring, the proposed on-line flutter monitoring test involves a temporal data-driven computation for the residual and builds on a different asymptotic for the residual, combined with the on-line cumulative sum (CUSUM) test of common use in quality control.

The paper is organized as follows. In next section is a summary of the main lines of the subspace-based monitoring residual investigated in earlier papers of the authors. The subsequent section is devoted to the design of the flutter monitoring test. In a first step, our previous detection method is applied to hypotheses adapted to the damping monitoring problem. Then a second design step handles different computation and approximation for the residual, which lead to the proposed on-line flutter monitoring test. The penultimate section is devoted to implementation issues and experimental results obtained on real data. Finally, some conclusions are drawn.

Subspace-Based Modal Identification and Monitoring

We first recall the models equations and parameters we use, and we recall the main lines of the subspace-based covariance-driven identification and monitoring algorithms that we advocate.

Modeling and Parameterizations

The use of state-space representations for modal analysis is well known,[11–13] and can be argued as follows. The structure's behavior is assumed to be described by a continuous time stationary linear system

$$M\ddot{\boldsymbol{\mathcal{Z}}}(t) + C\dot{\boldsymbol{\mathcal{Z}}}(t) + K\boldsymbol{\mathcal{Z}}(t) = \varepsilon(t), \qquad \boldsymbol{Y}(t) = L\boldsymbol{\mathcal{Z}}(t) \tag{1}$$

where M, C, and K are the mass, damping and stiffness matrices, respectively (high-dimensional), vector $\boldsymbol{\mathcal{Z}}$ collects the displacements of the degrees of freedom of the structure, the external (nonmeasured) force ε is modeled as a nonstationary white noise with time-varying covariance matrix $Q_\varepsilon(t)$, measurements are collected in the (often, low-dimensional) vector $\boldsymbol{Y}$, and matrix L indicates which components of the state vector are actually measured (where the sensors are located). The modes or eigenfrequencies denoted generically by μ and the modeshapes or eigenvectors denoted generically by Ψ_μ are solutions of

$$\det(\mu^2 M + \mu C + K) = 0, \qquad (\mu^2 M + \mu C + K)\Psi_\mu = 0 \tag{2}$$

Sampling model (1) at rate $1/\tau$ yields the discrete time model in state-space form,

$$\boldsymbol{X}_{k+1} = F\boldsymbol{X}_k + V_{k+1}, \qquad \boldsymbol{Y}_k = H\boldsymbol{X}_k \tag{3}$$

where the state and the output are

$$\boldsymbol{X}_k = \begin{pmatrix} \boldsymbol{\mathcal{Z}}(k\tau) \\ \dot{\boldsymbol{\mathcal{Z}}}(k\tau) \end{pmatrix}, \qquad \boldsymbol{Y}_k = \boldsymbol{Y}(k\tau) \tag{4}$$

the state transition and observation matrices are

$$F = e^{\mathcal{L}\tau}, \qquad \mathcal{L} = \begin{pmatrix} 0 & I \\ -M^{-1}K & -M^{-1}C \end{pmatrix}, \qquad H = (L \quad 0) \tag{5}$$

and state noise V_{k+1} is unmeasured, Gaussian, zero-mean, white, with covariance matrix

$$Q_{k+1} \overset{\text{def}}{=} \boldsymbol{E}\left(V_{k+1}V_{k+1}^T\right) = \int_{k\tau}^{(k+1)\tau} e^{\mathcal{L}s}\tilde{Q}(s)e^{\mathcal{L}^T s}\,\mathrm{d}s$$

where $\boldsymbol{E}(\,.\,)$ denotes the expectation operator and

$$\tilde{Q}(s) = \begin{pmatrix} 0 & 0 \\ 0 & M^{-1}Q_\varepsilon(s)(M^{-1})^T \end{pmatrix}$$

The whiteness assumption on V_{k+1} and the absence of measurement noise in Eqs. (3) are discussed in Ref. 14. It is stressed that sinusoidal or colored noise excitation can be encompassed as well. State $\boldsymbol{X}$ and observed output $\boldsymbol{Y}$ have dimensions $2m$ and r, respectively, with r (often much) smaller than $2m$ in practice.

Let (λ, ϕ_λ) be the eigenstructure of the state transition matrix F, namely,

$$\det(F - \lambda I) = 0, \qquad (F - \lambda I)\phi_\lambda = 0 \tag{6}$$

The modal parameters defined in Eqs. (2) are equivalently found from the eigenstructure $(\lambda, \varphi_\lambda)$ in Eqs. (6) using $e^{\tau\mu} = \lambda$ and $L\Psi_\mu = \varphi_\lambda \overset{\text{def}}{=} H\phi_\lambda$. The frequency f and damping coefficient ρ are recovered from a discrete eigenvalue λ through

$$f = a/2\pi\tau, \qquad \rho = 100|b|\Big/\sqrt{a^2 + b^2} \tag{7}$$

where $a = |\arctan \Im(\lambda)/\Re(\lambda)|$ and $b = \ell_n|\lambda|$. In the case where $C = \alpha M + \beta K$, the simplest form of proportional damping, the eigenvectors are real. Because of the structure of the state in Eq. (4), the λ and $\boldsymbol{\varphi}_\lambda$ are pairwise complex conjugate. We assume that the system has no multiple eigenvalues and that, in addition, 0 is not an eigenvalue of state transition matrix F. The collection of modes $(\lambda, \boldsymbol{\varphi}_\lambda)$ form a canonical parameterization, namely, a

parameterization invariant with respect to changes in the state basis, of the pole part of the system in Eqs. (3), referred to as the system eigenstructure. Note that the system eigenstructure can equally be found from the autoregressive (AR) part of a multivariable autoregressive moving average model equivalent to Eqs. (3) (Ref. 15), but that the AR vector parameters are not canonical. From now on, the collection of modes is also considered as the system parameter $\boldsymbol{\theta}$:

$$\boldsymbol{\theta} \stackrel{\text{def}}{=} \begin{pmatrix} \boldsymbol{\Lambda} \\ \text{vec}\Phi \end{pmatrix} \tag{8}$$

In Eq. (8), $\boldsymbol{\Lambda}$ is the vector whose elements are the eigenvalues λ, Φ is the matrix whose columns are the φ_λ, and vec is the column stacking operator. Parameter $\boldsymbol{\theta}$ has size $2m(r+1)$.

The measurement equation in Eqs. (3) with H as in Eq. (5) implicitly assumes that the available sensors measure the (relative) displacements of the degrees of freedom themselves, namely, are constraint gauges. If constraint gauges, velocity sensors, and accelerometers are available, the measurement equation in Eqs. (1) and observation matrix in Eqs. (4) should be

$$\boldsymbol{Y}(t) = \begin{pmatrix} L\mathcal{Z}(t) \\ N\dot{\mathcal{Z}}(t) \\ P\ddot{\mathcal{Z}}(t) \end{pmatrix}, \qquad H = \begin{pmatrix} L & 0 \\ 0 & N \\ -PM^{-1}K & -PM^{-1}C \end{pmatrix}$$

with L, N, P made of 0s and 1s. Consequently, state-space model (3) can always be enforced, whatever the sensors are. The nature of the sensors only influences the observation matrix H.

Residual Associated with Subspace Identification

The use of either covariance-driven or data-driven subspace-based identification algorithms for structural analysis has been discussed in Refs. 1 and 12. The use of the covariance-driven algorithm might be appealing when processing long samples of multisensor output measurements, which can be mandatory for in-operation structural analysis under nonstationary natural excitation. The data-driven subspace-based identification algorithms are discussed in Ref. 16. In this section, we describe the key steps of the output-only covariance-driven subspace structural identification method, and a characterization of the modal parameter in Eq. (8) is exhibited, from which the proposed residual is defined.

Covariance-Driven Subspace Identification

Let $R_i \stackrel{\text{def}}{=} \boldsymbol{E}(Y_k Y_{k-i}^T)$ and

$$\mathcal{H}_{p+1,q} \stackrel{\text{def}}{=} \begin{pmatrix} R_0 & R_1 & \vdots & R_{q-1} \\ R_1 & R_2 & \vdots & R_q \\ \vdots & \vdots & \vdots & \vdots \\ R_p & R_{p+1} & \vdots & R_{p+q-1} \end{pmatrix} \stackrel{\text{def}}{=} \text{Hank}\, R_i \tag{9}$$

be the output covariance and Hankel matrices, respectively. Introducing the cross covariance between the state and the observed outputs, $G \stackrel{\text{def}}{=} \boldsymbol{E}(X_k Y_k^T)$, direct computations of the R_i from Eqs. (3) lead to $R_i = HF^iG$ and to the well-known factorization

$$\mathcal{H}_{p+1,q} = \mathcal{O}_{p+1}(H,F)\mathcal{C}_q(F,G) \tag{10}$$

where

$$\mathcal{O}_{p+1}(H,F) \stackrel{\text{def}}{=} \begin{pmatrix} H \\ HF \\ \vdots \\ HF^p \end{pmatrix}, \mathcal{C}_q(F,G) \stackrel{\text{def}}{=} (G \quad FG \quad \cdots \quad F^{q-1}G) \tag{11}$$

are the observability and controllability matrices, respectively. The observation matrix H is then found in the first block row of the observability matrix $\mathcal{O}$. The state-transition matrix F is obtained from the shift invariance property of $\mathcal{O}$, namely, $\mathcal{O}_p^{\uparrow}(H,F) = \mathcal{O}_p(H,F)F$, where $\mathcal{O}_p^{\uparrow}(H,F)$ contains the last p block rows of $\mathcal{O}_{p+1}(H,F)$. Assuming $\text{rank}(\mathcal{O}_p) = \dim F$, and, thus, that the number of block rows in $\mathcal{H}_{p+1,q}$ is large enough, is mandatory for recovering F. The eigenstructure (λ, ϕ_λ) then results from Eqs. (6).

To handle an unmeasured measurement noise in Eqs. (3), modeled as a moving average (MA)(ι) Gaussian sequence with zero mean, a possible solution consists in filling the Hankel matrix in Eq. (9), starting with $R(\iota+1)$ instead of R_0. Here we use the notational convention that $\iota = -1$ for no measurement noise, and $\iota = 0$ for white independent identically distributed measurement noise. Note that, with this MA assumption, measurement noise does not affect the eigenstructure of system (3). Note also that such a handling of shifted covariances may be a solution for increasing the robustness with respect to the time lag effects produced by unsteady aerodynamics.

Modal Parameter Characterization and Monitoring Residual

Factorization (10) is the key for a characterization of the canonical parameter vector θ in Eq. (8) and for deriving the proposed residual. Choosing the eigenvectors of matrix F as a basis for the state space of model (3) yields the following modal representation of the observability matrix:

$$\mathcal{O}_{p+1}(\theta) = \begin{pmatrix} \Phi \\ \Phi\Delta \\ \vdots \\ \Phi\Delta^p \end{pmatrix} \tag{12}$$

where $\Delta \stackrel{\text{def}}{=} \text{diag}(\boldsymbol{\Lambda})$ and $\boldsymbol{\Lambda}$ and Φ are as in Eq. (8). Whether a nominal parameter $\boldsymbol{\theta}_0$ fits a given output covariance sequence $(R_j)_j$ is characterized by[13] that $\mathcal{O}_{p+1}(\boldsymbol{\theta}_0)$ and $\mathcal{H}_{p+1,q}$ have the same left kernel space. (The left kernel space of matrix M is the kernel space of matrix M^T.) This property can be checked as follows. From the nominal $\boldsymbol{\theta}_0$, compute $\mathcal{O}_{p+1}(\boldsymbol{\theta}_0)$ using matrix (12), and perform, for example, a singular value decomposition (SVD) of $\mathcal{O}_{p+1}(\boldsymbol{\theta}_0)$ to extract a matrix U such that $U^TU = I_s$ and $U^T\mathcal{O}_{p+1}(\boldsymbol{\theta}_0) = 0$. Matrix U is not unique. (Two such matrices relate through a post-multiplication with an orthonormal matrix.) However, matrix U can be regarded as a function of $\boldsymbol{\theta}_0$. Then the characterization is

$$U(\boldsymbol{\theta}_0)^T\mathcal{H}_{p+1,q} = 0 \tag{13}$$

Assume now that a reference $\boldsymbol{\theta}_0$ and a new sample $\boldsymbol{Y}_1, \ldots, \boldsymbol{Y}_n$ are available. To check whether the data agree with $\boldsymbol{\theta}_0$, the idea is to compute the empirical Hankel matrix $\hat{\mathcal{H}}_{p+1,q}$,

$$\hat{\mathcal{H}}_{p+1,q} \stackrel{\text{def}}{=} \text{Hank}\,(\hat{R}_i), \qquad \hat{R}_i \stackrel{\text{def}}{=} 1/(n-1)\sum_{k=i+1}^{n} \boldsymbol{Y}_k \boldsymbol{Y}_{k-i}^T \tag{14}$$

and to define the residual vector,

$$\zeta_n(\boldsymbol{\theta}_0) \stackrel{\text{def}}{=} \sqrt{n}\,\text{vec}\left[U(\boldsymbol{\theta}_0)^T\hat{\mathcal{H}}_{p+1,q}\right] \tag{15}$$

Let $\boldsymbol{\theta}$ be the actual parameter value for the system that generated the new data sample and $\boldsymbol{E}_\theta$ be the expectation when the actual system parameter is $\boldsymbol{\theta}$. From characterization (13), we know that $\boldsymbol{E}_\theta[\zeta_n(\boldsymbol{\theta}_0)] = 0$ iff $\boldsymbol{\theta} = \boldsymbol{\theta}_0$. In other words, $\zeta_n(\boldsymbol{\theta}_0)$ has zero mean when no change occurs in $\boldsymbol{\theta}$ and nonzero mean if a change occurs. Thus, $\zeta_n(\boldsymbol{\theta}_0)$ plays the role of a residual.

Onboard χ^2 test for Modal Monitoring

Testing if $\boldsymbol{\theta} = \boldsymbol{\theta}_0$ holds true or not, or equivalently deciding that residual ζ_n is significantly different from zero, requires the probability distribution of $\zeta_n(\boldsymbol{\theta}_0)$. Unfortunately, this distribution is generally unknown. A possible approach is to assume close hypotheses:

$$\text{(Safe)}\,\boldsymbol{H}_0 : \boldsymbol{\theta} = \boldsymbol{\theta}_0, \qquad \text{(Damaged)}\,\boldsymbol{H}_1 : \boldsymbol{\theta} = \boldsymbol{\theta}_0 + \delta\boldsymbol{\theta}\big/\sqrt{n} \tag{16}$$

where vector $\delta\theta$ is unknown but fixed. For large n, H_1 corresponds to small deviations in θ. This is the statistical local approach.[17–19] Define the mean deviation

$$\mathcal{J}(\theta_0) \stackrel{\text{def}}{=} -\frac{1}{\sqrt{n}}\frac{\partial}{\partial\theta}E_{\theta_0}\zeta_n(\theta)|_{\theta=\theta_0} \tag{17}$$

and the residual covariance matrix $\Sigma(\theta_0) \stackrel{\text{def}}{=} \lim_{n\to\infty} E_{\theta_0}(\zeta_n\zeta_n^T)$. Then, provided that $\Sigma(\theta_0)$ is positive definite, and for all $\delta\theta$ (including $\delta\theta = 0$), the residual ζ_n in Eq. (15) is asymptotically Gaussian distributed[13] when assuming θ as in Eq. (16):

$$\zeta_n(\theta_0) \xrightarrow[n\to\infty]{} \mathcal{N}[\mathcal{J}(\theta_0)\delta\theta,\ \Sigma(\theta_0)] \tag{18}$$

where $\mathcal{N}(\mu, \Sigma)$ stands for the Gaussian (normal) distribution with mean vector μ and covariance matrix Σ. Thus a deviation $\delta\theta \neq 0$ in the system parameter θ is reflected into a change in the mean value of residual ζ_n. Note that matrices $\mathcal{J}(\theta_0)$ and $\Sigma(\theta_0)$ depend on neither n nor the deviation $\delta\theta$. They can be estimated before testing, using data on the safe system, just as the reference θ_0. Consistent estimates of $\mathcal{J}$, based on a data sample, are given in Ref. 13 and do not depend on the particular normalization of the eigenvectors φ_λ. The estimation of Σ is somewhat tricky.[17]

Let $\hat{\mathcal{J}}$ and $\hat{\Sigma}$ be consistent estimates of $\mathcal{J}(\theta_0)$ and $\Sigma(\theta_0)$, and assume that $\mathcal{J}(\theta_0)$ is full column rank. Then, deciding whether residual ζ_n is significantly different from zero, stated as testing the presence of a small deviation in θ hypotheses (16), can be achieved with the aid of the generalized likelihood ratio (GLR) test based on the distribution (18), namely,

$$\begin{aligned}\sup_{\theta\in H_1}&\left[-(\zeta_n - \hat{\mathcal{J}}\delta\theta)^T\hat{\Sigma}^{-1}(\zeta_n - \hat{\mathcal{J}}\delta\theta)\right]\\ &- \sup_{\theta\in H_0}\left[-(\zeta_n - \hat{\mathcal{J}}\delta\theta)^T\hat{\Sigma}^{-1}(\zeta_n - \hat{\mathcal{J}}\delta\theta)\right]\\ &= \sup_{\delta\theta\neq 0}\left[-(\zeta_n - \hat{\mathcal{J}}\delta\theta)^T\hat{\Sigma}^{-1}(\zeta_n - \hat{\mathcal{J}}\delta\theta)\right] + \zeta_n\hat{\Sigma}^{-1}\zeta_n\end{aligned} \tag{19}$$

This boils down to the following χ^2 test:

$$\chi_n^2(\theta_0) \stackrel{\text{def}}{=} \zeta_n^T(\theta_0)\hat{\Sigma}^{-1}\hat{\mathcal{J}}(\hat{\mathcal{J}}^T\hat{\Sigma}^{-1}\hat{\mathcal{J}})^{-1}\hat{\mathcal{J}}^T\hat{\Sigma}^{-1}\zeta_n(\theta_0) \tag{20}$$

which should be compared to a threshold. Note that the only term in Eq. (20) that is computed when collecting fresh data is $\zeta_n(\theta_0)$. Test $\chi_n^2(\theta_0)$ is asymptotically distributed as a χ^2 variable, with $\text{rank}(\mathcal{J})$ degrees of freedom and noncentrality parameter under H_1: $\delta\theta^T\mathcal{J}(\theta_0)^T\Sigma(\theta_0)^{-1}\mathcal{J}(\theta_0)\delta\theta$. In other words,

$$\begin{aligned}E_{H_0}\chi_n^2(\theta_0) &= \text{rank}[\mathcal{J}(\theta_0)]\\ E_{H_1}\chi_n^2(\theta_0) &= \text{rank}[\mathcal{J}(\theta_0)] + \delta\theta^T\mathcal{J}(\theta_0)^T\Sigma(\theta_0)^{-1}\mathcal{J}(\theta_0)\delta\theta\end{aligned} \tag{21}$$

In practice, however, the actual values of χ_n^2 are much higher than those theoretical ones. How to select a threshold for χ_n^2 from histograms of empirical values obtained on data for undamaged cases is explained in Ref. 20. Other application examples are described in Ref. 21.

For numerical efficiency, it may be preferable to normalize the residual to handle identity covariance matrices for all parameter values θ_0. For this purpose, we introduce the scale-normalized residual

$$\bar{\zeta}_n(\theta_0) \stackrel{\text{def}}{=} \mathcal{J}(\theta_0)^T\Sigma(\theta_0)^{-1}\zeta_n(\theta_0) \tag{22}$$

and the covariance matrix

$$\bar{\Sigma}(\theta_0) \stackrel{\text{def}}{=} \mathcal{J}(\theta_0)^T\Sigma(\theta_0)^{-1}\mathcal{J}(\theta_0) \tag{23}$$

It results from distribution (18) that $\bar{\zeta}_n(\theta_0)$ is asymptotically Gaussian,

$$\bar{\zeta}_n(\theta_0) \xrightarrow[n\to\infty]{} \mathcal{N}[\bar{\Sigma}(\theta_0)\delta\theta,\ \bar{\Sigma}(\theta_0)] \tag{24}$$

and that $\bar{\Sigma}(\theta_0)^{-1/2}\bar{\zeta}_n(\theta_0)$ has asymptotical identity covariance matrix.

Modal Diagnosis

The modal diagnosis problem is to decide which components of θ have changed. Determining which eigenfrequencies and associated mode shapes have been affected by the damage is often addressed as an estimation problem, based on modal identification in the pre- and postdamage stages.[22] We address modal diagnosis as a detection problem instead, using the estimated Jacobian matrix $\hat{\mathcal{J}}_i$ corresponding to mode and mode shape i (Ref. 23). The directional test focused on this mode i is

$$\chi_n^{(i)2} \stackrel{\text{def}}{=} \zeta_n^T\hat{\Sigma}^{-1}\hat{\mathcal{J}}_i\left(\hat{\mathcal{J}}_i^T\hat{\Sigma}^{-1}\hat{\mathcal{J}}_i\right)^{-1}\hat{\mathcal{J}}_i^T\hat{\Sigma}^{-1}\zeta_n \tag{25}$$

Such a directional test restricted to the damping coefficient ρ of a given mode defined in Eqs. (7) could be seen as a solution to the flutter monitoring problem. However, the relevant hypotheses for that problem should be one sided (because one is interested in detecting a decrease in the damping), which is not the case in hypotheses (16). This calls for a further step in the design of a flutter monitoring test, as described next. In what follows, the caret above $\mathcal{J}$ and Σ are dropped for simplicity.

Flutter Monitoring

As explained in the Introduction, one manner to address the flutter problem is to decide whether some damping coefficient ρ decreases below some specified critical value ρ_c, namely, $\rho < \rho_c$. In this section, we describe a first step for solving this problem. It consists in applying the described approach to local hypotheses adapted to $\rho < \rho_c$. We assume that $\rho_c = \rho_0$, where ρ_0 is the actual value of the monitored damping coefficient, in the reference parameter θ_0. The realistic case $\rho_c < \rho_0$ is the topic of current investigations.

First Step, Working Batchwise

As before, the observed data are considered to consist of the residual $\zeta_n \stackrel{\text{def}}{=} \zeta_n(\theta_0)$ defined in Eq. (15).

Monitoring a Damping Coefficient

Let $\mathcal{J} \stackrel{\text{def}}{=} \mathcal{J}(\rho_0)$ be the Jacobian matrix corresponding to the damping coefficient ρ_0, and let $\Sigma \stackrel{\text{def}}{=} \Sigma(\theta_0)$ be the residual covariance matrix. Because ρ_0 is a scalar number, the matrix $\mathcal{J}$ is in fact a column vector, obtained by selecting the corresponding column of the matrix that results from the multiplication of $\mathcal{J}(\theta_0)$ with the Jacobian of the transformation (7) from the λ to the ρ (Ref. 23). For reasons explained earlier, one can equivalently handle the scale-normalized residual $\bar{\zeta}_n$ defined in Eq. (22), which now is

$$\bar{\zeta}_n(\rho_0) \stackrel{\text{def}}{=} \mathcal{J}(\rho_0)^T\Sigma(\theta_0)^{-1}\zeta_n(\theta_0) \tag{26}$$

and the covariance matrix

$$\bar{\Sigma}(\rho_0) \stackrel{\text{def}}{=} \mathcal{J}(\rho_0)^T\Sigma(\theta_0)^{-1}\mathcal{J}(\rho_0) \tag{27}$$

Note that $\bar{\zeta}_n(\rho_0)$ and $\bar{\Sigma}(\rho_0)$ are now scalar numbers and, moreover, that $\bar{\Sigma}(\rho_0) > 0$. It results from distribution (24) that, when assuming $\rho = \rho_0 + \delta\rho/\sqrt{n}$, for all $\delta\rho$,

$$\bar{\zeta}_n(\rho_0) \xrightarrow[n\to\infty]{} \mathcal{N}[\bar{\Sigma}(\rho_0)\delta\rho,\ \bar{\Sigma}(\rho_0)] \tag{28}$$

A deviation in ρ is, thus, reflected by a deviation of the same sign in the mean of $\bar{\zeta}_n(\rho_0)$.

Possible One-Sided Test

Consider now the following local hypotheses:

$$H_0 : \delta\rho \geq 0, \qquad H_1 : \delta\rho < 0 \tag{29}$$

which express that the damping coefficient decreases below ρ_0 while remaining in close neighborhoods. The GLR test for the testing problem (29), namely,

$$\begin{aligned}l_n(\rho_0) \stackrel{\text{def}}{=} &\sup_{\delta\rho<0}\left[-(\bar{\zeta}_n - \bar{\Sigma}\delta\rho)^T\bar{\Sigma}^{-1}(\bar{\zeta}_n - \bar{\Sigma}\delta\rho)\right]\\ &- \sup_{\delta\rho\geq 0}\left[-(\bar{\zeta}_n - \bar{\Sigma}\delta\rho)^T\bar{\Sigma}^{-1}(\bar{\zeta}_n - \bar{\Sigma}\delta\rho)\right]\end{aligned}$$

can be shown[24] to reduce to

$$l_n(\rho_0) = -\text{sign}\,[\bar{\zeta}_n(\rho_0)] \cdot \bar{\chi}_n^2(\rho_0)$$

$$\bar{\chi}_n^2(\rho_0) \stackrel{\text{def}}{=} \bar{\zeta}_n(\rho_0)^T \bar{\Sigma}(\rho_0)^{-1} \bar{\zeta}_n(\rho_0) \tag{30}$$

The test statistics $l_n(\rho_0)$ satisfies the following property: $\boldsymbol{E}_{H_0} l_n(\rho_0) \leq 0$ and $\boldsymbol{E}_{H_1} l_n(\rho_0) > 0$. In other words, it manifests the change in $\delta\rho$ by a change in the sign of its own mean. Thus, it is a good candidate for solving the hypotheses testing problem (29). A decision in favor of $\boldsymbol{H}_1$ can be made when $l_n(\rho_0) \geq \gamma$, for some positive threshold γ to be chosen.

It turns out that the online adaptation of this basically off-line test is about as computationally complex as the identification algorithm itself. Consequently, this test does not provide us with an answer to the online monitoring problem.

Second Step, Working Online

Now, a further step is taken toward designing an online flutter monitoring algorithm. Another decision function is introduced, which builds on a different computation for the same scale-normalized residual $\bar{\zeta}_n(\rho_0)$ as in residual (26) no longer covariance driven but now temporal data driven. It also builds on a different approximation for $\bar{\zeta}_n(\rho_0)$ and on the CUSUM test statistics.[18]

Another Insight in the Residual

Because of Eq. (15), the residual (26) is

$$\bar{\zeta}_n(\rho_0) = \sqrt{n}\, \mathcal{J}(\rho_0)^T \Sigma(\boldsymbol{\theta}_0)^{-1} \text{vec}\big[U(\boldsymbol{\theta}_0)^T \hat{\mathcal{H}}_{p+1,q}\big] \tag{31}$$

Because of Eq. (14), and assuming $n > p + q$, this is rewritten as

$$\bar{\zeta}_n(\rho_0) = \sum_{k=q}^{n-p} \frac{\boldsymbol{Z}_k(\rho_0)}{\sqrt{n}} \tag{32}$$

where

$$\boldsymbol{Z}_k(\rho_0) \stackrel{\text{def}}{=} \mathcal{J}(\rho_0)^T \Sigma(\boldsymbol{\theta}_0)^{-1} \text{vec}\left[U(\boldsymbol{\theta}_0)^T \mathcal{Y}^+_{k,p+1} \mathcal{Y}^{-\,T}_{k,q}\right] \tag{33}$$

$$\mathcal{Y}^+_{k,p+1} \stackrel{\text{def}}{=} \begin{pmatrix} \boldsymbol{Y}_k \\ \vdots \\ \boldsymbol{Y}_{k+p} \end{pmatrix}, \qquad \mathcal{Y}^-_{k,q} \stackrel{\text{def}}{=} \begin{pmatrix} \boldsymbol{Y}_k \\ \vdots \\ \boldsymbol{Y}_{k-q+1} \end{pmatrix}$$

From distribution (24), we know that $\bar{\zeta}_n(\rho_0)$, and thus,

$$\sum_{k=q}^{n-p} \frac{\boldsymbol{Z}_k(\rho_0)}{\sqrt{n}}$$

is asymptotically Gaussian distributed, with zero mean under the hypothesis $\rho = \rho_c$. Now, the following approximation results from the arguments in Ref. 25: For k large enough, $\boldsymbol{Z}_k(\rho_0)$ is asymptotically Gaussian distributed, with zero mean under $\rho = \rho_c$, and the $\boldsymbol{Z}_k(\rho_0)$ are independent. Furthermore, as already mentioned, a change from $\rho \geq \rho_c$ to $\rho < \rho_c$ is reflected by a decrease in the mean value ν of $\boldsymbol{Z}_k(\rho_0)$.

CUSUM Test

Consider now the following nonlocal hypotheses concerning the mean value ν of the independent Gaussian variables $\boldsymbol{Z}_k$:

$$\tilde{\boldsymbol{H}}_0 : \nu \geq 0, \qquad \tilde{\boldsymbol{H}}_1 : \nu < 0 \tag{34}$$

Testing between these hypotheses can be addressed with the aid of the CUSUM test in common use in quality control and defined as follows[18]:

$$S_n(\rho_0) \stackrel{\text{def}}{=} \bar{\Sigma}(\boldsymbol{\theta}_0)^{-\frac{1}{2}} \sum_{k=q}^{n-p} \boldsymbol{Z}_k(\rho_0) \tag{35}$$

$$T_n(\rho_0) \stackrel{\text{def}}{=} \max_{q \leq k \leq n-p} S_k(\rho_0)$$

$$g_n(\rho_0) \stackrel{\text{def}}{=} T_n(\rho_0) - S_n(\rho_0) \tag{36}$$

The test statistics $g_n(\rho_0)$ enjoy the following properties: $\boldsymbol{E}_{\tilde{H}_0} g_n(\rho_0) \approx 0$ and $\boldsymbol{E}_{\tilde{H}_1} g_n(\rho_0) > 0$. A decision in favor of $\tilde{\boldsymbol{H}}_1$ is made when $g_n(\rho_0) \geq \gamma$, for some threshold γ to be chosen. Note that g_n monitors online the deviations of the CUSUM S_n with respect to its maximum value T_n. In other words, the sum is confronted with an adaptive threshold: $S_n \leq T_n - \gamma$.

Now, from Eqs. (32), (33), and (35), we have $S_n(\rho_0) = \bar{\Sigma}(\boldsymbol{\theta}_0)^{-1/2}[\sqrt{n}\bar{\zeta}_n(\rho_0)]$, from which we deduce that test g_n in Eq. (36) handles the time-unnormalized residual $\bar{\zeta}_n(\rho_0)$.

Proposed Online Flutter Test

Because neither what is the actual hypothesis when this processing starts nor what are the actual sign and magnitude of the change in ρ that will occur are known, a relevant procedure[18] consists of the following steps:

1) Introduce a minimum magnitude of change $\nu_m > 0$, namely, test between

$$\tilde{\boldsymbol{H}}_0 : \nu \geq +\nu_m/2 \qquad \text{and} \qquad \tilde{\boldsymbol{H}}_1 : \nu < -\nu_m/2 \tag{37}$$

and vice versa.

2) Run two tests in parallel, for a decreasing and an increasing damping, respectively.

3) Make a decision according to the first test statistics that crosses its threshold.

4) Switch to the other one afterward.

At a first glance, having to tune an additional parameter may appear as a drawback. It turns out, however, that the choices of the minimum magnitude ν_m and of the threshold γ are generally well decoupled.[18] See the discussion in the next section.

This algorithm is summarized as follows. (The dependency in $\boldsymbol{\theta}_0$ and ρ_0 is dropped.)

Decreasing damping:

$$S_n^{(-)} \stackrel{\text{def}}{=} \bar{\Sigma}^{-\frac{1}{2}} \sum_{k=q}^{n-p} (Z_k + \nu_m), \qquad T_n^{(-)} \stackrel{\text{def}}{=} \max_{q \leq k \leq n-p} S_k^{(-)}$$

$$g_n^- \stackrel{\text{def}}{=} T_n^{(-)} - S_n^{(-)}, \qquad g_n^- \geq \gamma^- \tag{38}$$

Increasing damping:

$$S_n^{(+)} \stackrel{\text{def}}{=} \bar{\Sigma}^{-\frac{1}{2}} \sum_{k=q}^{n-p} (Z_k - \nu_m), \qquad T_n^{(+)} \stackrel{\text{def}}{=} \min_{q \leq k \leq n-p} S_k^{(+)}$$

$$g_n^+ \stackrel{\text{def}}{=} S_n^{(+)} - T_n^{(+)}, \qquad g_n^+ \geq \gamma^+ \tag{39}$$

When $g_n^- \geq \gamma^-$, both CUSUMs $S_n^{(-)}$ and $S_n^{(+)}$ and both extrema $T_n^{(-)}$ and $T_n^{(+)}$ are reset to zero, and g_n^+ is activated. When $g_n^+ \geq \gamma^+$, both CUSUMs $S_n^{(-)}$ and $S_n^{(+)}$ and both extrema are reset to zero, and g_n^- is activated. Let t_i, $i = 1, \ldots,$ be the alarm and switch time instants. The actual test statistics h_t corresponding to this processing and plotted in Figs. 1 and 2, is defined by

$$\forall t \in [t_k, t_{k+1}]$$

$$h_t \stackrel{\text{def}}{=} \begin{cases} +g_t^+ & \text{if} \quad h_t \equiv -g_t^- \quad \forall t \in [t_{k-1}, t_k] \\ -g_t^- & \text{if} \quad h_t \equiv +g_t^+ \quad \forall t \in [t_{k-1}, t_k] \end{cases} \tag{40}$$

Because the test statistics g_n^- monitors a drop in the damping, $h_t = -g_t^-$ is plotted in gray (bottom) to better visualize a drop. Similarly, because the test statistics g_n^+ monitors an increase in the damping, $h_t = g_t^+$ is plotted in black (top). We stress that $\|h_t\|$ is small when $\rho \gg \rho_c$ and large when ρ is close to, or crosses, ρ_c. When Figs. 1 and 2 are examined, note this intuitively desirable and very useful property.

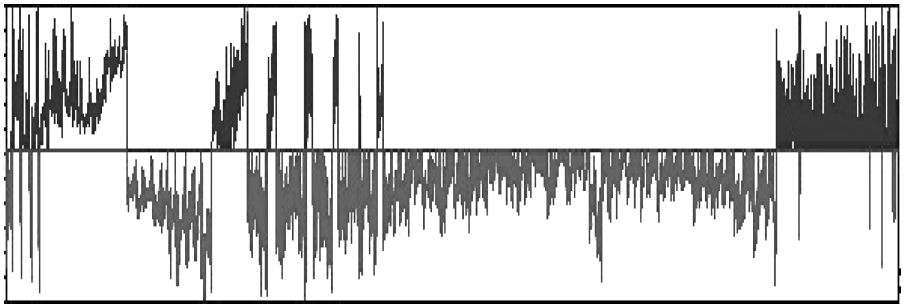

Fig. 1 Test h_t for $\rho_c = \rho_c^{(1)}$; X axis is time (seconds), test run samplewise: bottom, $-g_n^-$ reflects $\rho < \rho_c$ and top, g_n^+ reflects $\rho > \rho_c$.

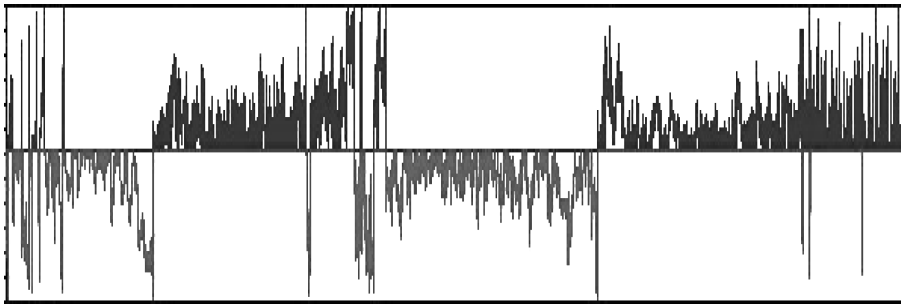

Fig. 2 Test h_t for $\rho_c = \rho_c^{(2)} < \rho_c^{(1)}$; reflects $\rho > \rho_c$. X axis is time (seconds), test run samplewise: bottom, $-g_n^-$ reflects $\rho < \rho_c$ and top g_n^+ reflects $\rho > \rho_c$.

Application

In this section, we discuss some implementation and tuning issues related to the online detection algorithm, and we present numerical results obtained with a real application example.

Implementation and Tuning Issues

Automatic modal analysis and monitoring one damping coefficient have been performed using the Scilab modal analysis and damage detection and localization toolbox. (The toolbox can be downloaded from http://www.irisa.fr/sigma2/constructif/modal.htm.)

Note that the proposed flutter monitoring algorithm (40) can be computed in real time, whereas automatic modal identification is both computationally expensive and subject to estimation errors, especially in the damping factors. Actually, the proposed damping test does not require reidentification of the damping coefficient at every step. Thus, it is much faster and free from estimation error propagation. To tune this algorithm, the user has to choose a minimum magnitude of change ν_m and a threshold γ. This should be done by extensive manual training, which has not been possible in the present example due to lack of reference data, and can be achieved based on the following remarks:

1) The threshold γ should be high enough to avoid reactions to small fluctuations and small enough to allow quick detection and avoid missed detection of damping changes.

2) The minimum magnitude of change ν_m should be chosen close to zero. A zero value leads to a flutter test with high fluctuations around the critical damping value. Increasing the value of ν_m introduces a dead zone between the two hypotheses (37) and, thus, removes false alarms. However, too high a ν_m prevents the test from reacting.

Real Application Example

The tests statistics h_t, defined by algorithms (38–40), has been applied to a data set provided by the European Aeronautic Defence and Space Company (EADS) Space Transportation. The data have been collected on the Ariane booster launcher during a launch scenario on the ground (not during a real flight test). The structure and the data are highly nonstationary because of propellant consumption. Moreover, the structure is subject to unmeasured excitation due to turbulence. Also, various controlled observed excitations have been applied in a switching manner. These excitations are neither used nor even available for our numerical experimentations. Such a change in the controlled excitation (and not the structure's evolution) explains the first peak in the damping plot (Fig. 3).

The data have been bandpass filtered to focus on one particular frequency band. A preliminary analysis of the data led us to select a small subset of sensors for monitoring the mode of interest. Using more sensors would have yielded, first, a loss of quality in the estimation, and, second, a loss in the observability of the considered mode. Identification and testing have been performed with the same subset of sensors. Because the data are highly nonstationary, a 5-s sliding window with overlap has been used for the identification.

Our main purpose in applying the proposed test to those data is to check whether we can monitor one specific mode during a short (typically less than 1 min) but quickly changing period. Focusing on one specific mode is not a limitation of the method: The algorithm can be modified to handle several modes simultaneously. Our purpose with the test is also to match as much as possible the results of subspace-based identification (recognized as a bench), with a lower computational cost, to the extent of several orders of magnitude.

Experimental Results

The results of the automatic modal analysis for the considered mode are shown in Fig. 3. For obvious reasons, the actual values of the damping coefficient and the frequency cannot be shown. It appears clearly that, whereas the frequency is slowly increasing, the damping coefficient exhibits large fluctuations. The variations in the modal parameters are due to the mass loss, due to propellant consumption, which is not at all negligible. A statistical explanation for the different behavior of the frequency and of the damping is that damping factors are more difficult to estimate accurately than frequencies.[10] At the end of the sequence, the damping rises abnormally, and then the mode disappears from the spectrum of the considered sensors. The key point is that the real data set exhibits, on the estimation plot, a fluctuating damping coefficient, which makes it a good candidate for applying the proposed online detection algorithm. The goal here is to match as much as possible the results of subspace-based identification (recognized as a bench), using a detection algorithm with a lower computational cost, to the extent of several orders of magnitude.

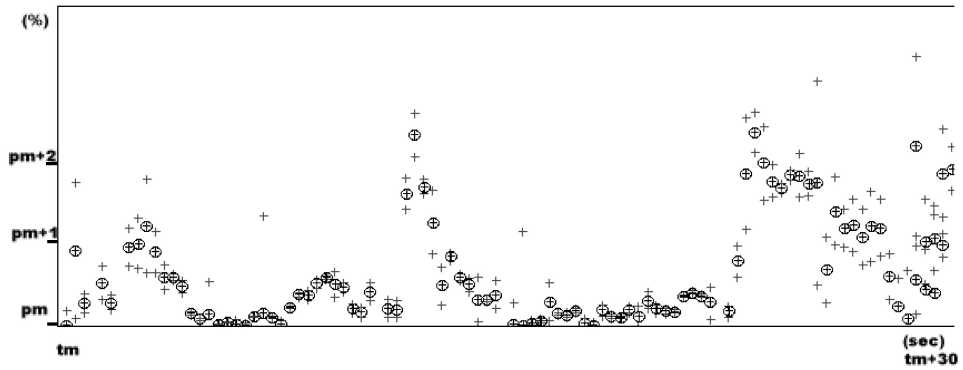

a) Dampings

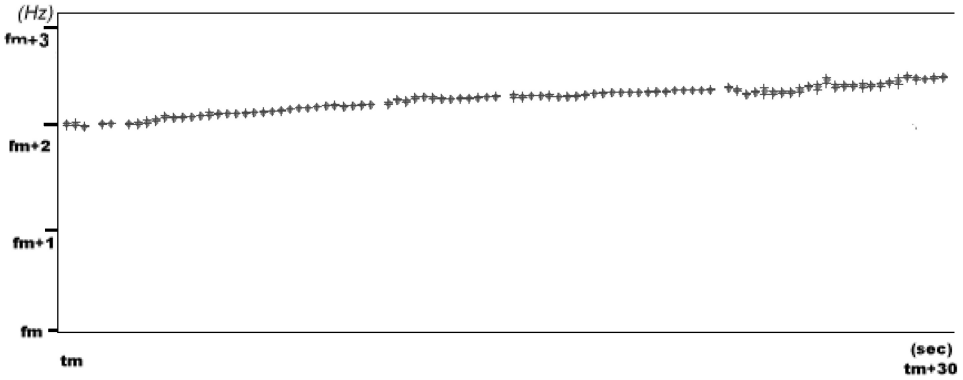

b) Frequencies

Fig. 3 Automatic identification of one frequency (hertz) and damping coefficient (%): *X* axis is time (seconds); symbol corresponds to processing of a data window (5 s, sampling frequency 400 Hz).

In Figs. 1 and 2, the behavior of the test statistics h_t in algorithms (40) is shown for two different values of the critical damping, $\rho_c = \rho_0 = \rho_c^{(1)}$ and $\rho_c^{(2)}$, with $\rho_c^{(2)} < \rho_c^{(1)}$. Note that the time axis is not exactly the same for Figs. 1 and 2 as for Fig. 3. This is because of batch processing for the latter and online samplewise processing for the two present figures. The lower quality of the results in the early, left parts of Figs. 1 and 2 can be explained as follows. The statistics g_n is a CUSUM, and the test relies on some kind of law of large numbers. (The empirical mean converges to a limit as the sample size increases.) Such a CUSUM has no real meaning at its early stage. A similar argument holds for in the early (left) portion of the identification plots in Fig. 3, where the higher damping values may be explained by the launch procedure. Nevertheless, it is clear that the time intervals during which alarms are fired (Fig. 1 and 2 bottoms statistics crossing its threshold) mainly correspond to the intervals in Fig. 3 with low damping values.

In Figs. 1 and 2, the tests show a coherent behavior. If the test in Fig. 2 indicates that the damping value is below $\rho_c^{(2)}$ (then it is gray), then the test in Fig. 1 also indicates the damping value below $\rho_c^{(1)}$ (it is also gray). Similar conclusions hold vice versa. This does not mean that Fig. 2 would imply Fig. 1. Running the two tests in parallel, we can consider that the damping lies between $\rho_c^{(2)}$ and $\rho_c^{(1)}$, as long as the plot is gray in Fig. 1 and black in Fig. 2, notwithstanding the left-hand side part of the plot. Note also that, when the test in Fig. 2 leaves its gray part, the test in Fig. 1 is still reacting, and leaves the gray part a bit later. Again similar conclusions hold vice versa (from the black part to the gray one). This is another coherence. A lack of coherence, with respect to the actual damping value, would be that the first test would not react while the second one reacts, whereas the damping is lower than both critical values, or that the second test would react while the first one is not reacting, whereas the damping is greater than both critical values. It turns out that this does not happen.

Discussion

Some further comments are in order, first on the advantages and drawbacks of the identification and online detection approaches, then on monitoring multiple damping coefficients, and finally on handling the more realistic case $\rho_c < \rho_0$.

Typically, identification would 1) require a larger amount of computing resources and 2) introduce possible estimation errors at each step of the flight. The proposed detection technique does not suffer from these drawbacks. However, it suffers from the calibration issue, namely, the estimation of the residual covariance matrix, which ideally requires a long data set. This is the price to be paid for assessing deviations significant with respect to noises and uncertainties. However, once this matrix is computed, the detection test is much more robust to time lag effects produced by unsteady aerodynamics than identification. Actually, during an identification procedure, the user has to balance records long enough for the identification against too long records suffering from the nonstationary effects, for example, unsteady aerodynamics. This is the tradeoff between bad estimates (bias) and fluctuating estimates (variance), a well-known identification issue. We stress that the proposed detection technique suffers from those drawbacks to a lower extent because 1) it performs detection without identification, and 2) it runs samplewise. Having consistent results between identification and detection plots leads us to conclude that both were done correctly. Identification and detection as presented in this paper should be considered as complementary approaches to the problem of monitoring a damping coefficient.

Monitoring multiple damping coefficients can be achieved by either running the corresponding tests in parallel (possibly with different values for the threshold γ and magnitude ν_m) or taking into account a multicolumn Jacobian in the test. Different values of ν_m for each of the two CUSUM tests g_n^- and g_n^+ could also be used for multiple testing. The rationale is as follows. A small change magnitude ν_m for test g_n^+ is likely to be relevant for an

instantaneous reaction when ρ crosses the damping value ρ_c from above and toward zero. On the contrary, a larger ν_m should be used to ensure that the decision in favor of the safe hypothesis $\rho > \rho_c$ is correct with high probability.

This type of tuning could also be used for handling the more realistic case $\rho_c < \rho_0$. In that case, one might try to tune ν_m to make the test react at the desired critical value ρ_c. Using a modal to data simulator to generate the (missing) data set at the critical value might also be useful. This is the topic of current investigations to be reported elsewhere.

Conclusions

Motivated by the flutter monitoring problem, we have described a statistical approach towards fast in-flight onboard detection of flutter onset. This approach combines modal model-based and in-flight data-based methods. The key elements in the design of an online statistical detection algorithm for monitoring a damping coefficient have been presented. The proposed test handles an output-only subspace-based residual previously proposed by the authors for both modal identification and SHM. Even though mode shapes are not monitored, they are explicitly involved in the computation of the proposed test. It is our experience that this may be of crucial importance in SHM, especially when detecting small deviations in the modal behavior. Whereas our SHM subspace-based residual was covariance driven and our SHM test was based on the asymptotic statistical local approach to monitoring, the online flutter monitoring test involves a temporal data-driven computation for the subspace-based residual and builds on a different asymptotic for the residual, combined with the online CUSUM test commonly used in quality control. We stress that the proposed detection technique performs detection without identification and runs samplewise and, consequently, partly overcomes the drawbacks resulting from the bias/variance tradeoff issue.

On a data set from a real nonstationary flight structure, the proposed subspace-based test has been shown to provide results that are both coherent with subspace-based identification results and promising from an online detection point of view.

Acknowledgments

This work has been carried out within the framework of Eureka Project 2419 FLITE (data available at URL: http://www.irisa.fr/sigma2/flite/), coordinated by Sopemea, Velizy-Villacoublay, France. This project aims at improving the exploitation of flight test data, to enable more direct exploration of the flight domain, with improved confidence and at reduced cost. The authors acknowledge the contribution of Benoit Ryckelynck (EADS SPACE Transportation) and Luc Gonidou (Centre National d'Etudes Spatiales) for providing the real data sets and for useful discussions. The contribution of Auguste Sam to the experimental results is acknowledged. The authors are indebted to the Associate Editor and the three referees, whose careful reading and detailed comments helped to improve an earlier version of the paper.

References

[1]Basseville, M., Benveniste, A., Goursat, M., Hermans, L., Mevel, L., and Van der Auweraer, H., "Output-Only Subspace-Based Structural Identification: From Theory to Industrial Testing Practice," *Journal of Dynamic Systems Measurement and Control*, Vol. 123, No. 4, 2001, pp. 668–676.

[2]Mevel, L., Goursat, M., and Benveniste, A., "Using Subspace on Flight Data, a Practical Example," *Proceedings of the Twenty-First International Modal Analysis Conference* [CD-ROM], Society for Experimental Mechanics, Paper 138, 2003.

[3]Kehoe, M. W., "A Historical Overview of Flight Flutter Testing," NASA TM-4720, Oct. 1995.

[4]Pickrel, C. R., and White, P. J., "Flight Flutter Testing of Transport Aircraft: In-Flight Modal Analysis," *Proceedings of the Twenty-First International Modal Analysis Conference* [CD-ROM], Society for Experimental Mechanics, Paper 200, 2003.

[5]Lind, R., "Flight-Test Evaluation of Flutter Prediction Methods," *Journal of Aircraft*, Vol. 40, No. 5, 2003, pp. 964–970.

[6]Dimitriadis, G., and Cooper, J. E., "Flutter Prediction from Flight Flutter Test Data," *Journal of Aircraft*, Vol. 38, No. 2, 2001, pp. 355–367.

[7]Feron, E., Brenner, M. J., Paduano, J., and Turevskiy, A., "Time-Frequency Analysis for Transfer Function Estimation and Application to Flutter Clearance," *Journal of Guidance, Control, and Dynamics*, Vol. 21, No. 3, 1998, pp. 375–382.

[8]Verboven, P., Cauberghe, B., Guillaume, P., Vanlanduit, S., and Parloo, E., "Modal Parameter Estimation and Monitoring for On-Line Flight Flutter Analysis," *Mechanical Systems and Signal Processing*, Vol. 18, No. 3, 2004, pp. 587–610.

[9]Lind, R., and Brenner, M., "Flutterometer: An On-Line Tool to Predict Robust Flutter Margins," *Journal of Aircraft*, Vol. 37, No. 6, 2000, pp. 1105–1112.

[10]Gersch, W., "On the Achievable Accuracy of Structural Parameter Estimates," *Journal Sound and Vibration*, Vol. 34, No. 1, 1974, pp. 63–79.

[11]Juang, J. N., *Applied System Identification*, Prentice–Hall, Englewood Cliffs, NJ, 1994.

[12]Peeters, B., and De Roeck, G., "Reference-Based Stochastic Subspace Identification for Output-Only Modal Analysis," *Mechanical Systems and Signal Processing*, Vol. 13, No. 6, 1999, pp. 855–878.

[13]Basseville, M., Abdelghani, M., and Benveniste, A., "Subspace-Based Fault Detection Algorithms for Vibration Monitoring," *Automatica*, Vol. 36, No. 1, 2000, pp. 101–109.

[14]Mevel, L., Basseville, M., Benveniste, A., and Goursat, M., "Merging Sensor Data from Multiple Measurement Setups for Nonstationary Subspace-Based Modal Analysis," *Journal Sound and Vibration*, Vol. 249, No. 3, 2002, pp. 719–741.

[15]Akaïke, H., "Markovian Representation of Stochastic Processes and Its Application to the Analysis of Autoregressive Moving Average Processes," *Annals of the Institute of Statistical Mathematics*, Vol. 26, No. 2, 1974, pp. 363–387.

[16]Van Overschee, P., and De Moor, B., *Subspace Identification for Linear Systems: Theory—Implementation—Methods*, Kluwer, Dordrecht, The Netherlands, 1996.

[17]Zhang, Q., Basseville, M., and Benveniste, A., "Early Warning of Slight Changes in Systems and Plants with Application to Condition Based Maintenance," *Automatica*, Vol. 30, No. 1, 1994, pp. 95–114.

[18]Basseville, M., and Nikiforov, I. V., *Detection of Abrupt Changes—Theory and Application*, Prentice–Hall, Englewood Cliffs, NJ, 1993, Chaps. 2, 4, 10, 11; also available at URL: http://www.irisa.fr/sigma2/kniga/ [cited November 1998].

[19]Basseville, M., "On-Board Component Fault Detection and Isolation Using the Statistical Local Approach," *Automatica*, Vol. 34, No. 11, 1998, pp. 1391–1416.

[20]Mevel, L., Goursat, M., and Basseville, M., "Stochastic Subspace-Based Structural Identification and Damage Detection and Localization—Application to the Z24 Bridge Benchmark," *Mechanical Systems and Signal Processing*, Vol. 17, No. 1, 2003, pp. 143–151.

[21]Mevel, L., Hermans, L., and Van der Auweraer, H., "Application of a Subspace-Based Fault Detection Method to Industrial Structures," *Mechanical Systems and Signal Processing*, Vol. 13, No. 6, 1999, pp. 823–838.

[22]Farrar, C. R., Doebling, S. W., and Nix, D. A., "Vibration-Based Structural Damage Identification," *Royal Society, Philosophical Transactions: Mathematical, Physical and Engineering Sciences*, Vol. 359, No. 1778, 2001, pp. 131–150.

[23]Basseville, M., Mevel, L., and Goursat, M., "Statistical Model-Based Damage Detection and Localization: Subspace-Based Residuals and Damage-to-Noise Sensitivity Ratios," *Journal Sound and Vibration* (to be published); also available at URL: http://www.sciencedirect.com [cited 27 October 2003].

[24]Lehmann, E. L., *Testing Statistical Hypotheses*, 2nd ed., Springer, New York, 1986.

[25]Benveniste, A., Métivier, M., and Priouret, P., *Adaptive Algorithms and Stochastic Approximations*, Springer, New York, 1990, Chap. 5.4.1.